

A Meshless, Spectrally Accurate, Integral Equation Solver for Molecular Surface Electrostatics

SHIH-HSIEN KUO, BRUCE TIDOR, and JACOB WHITE
 Massachusetts Institute of Technology

The need to determine electrostatic fields in domains bounded by molecular surfaces arises in a number of nanotechnology applications including: biomolecule design, carbon nanotube simulation, and molecular electron transport analysis. Molecular surfaces are typically smooth, without the corners common in electrical interconnect problems, but are often so geometrically complicated that numerical evaluation of the associated electrostatic fields is extremely time-consuming. In this paper we describe and demonstrate a meshless spectrally-accurate integral equation method that *only* requires a description of the molecular surface in the form of a collection of surface points. Our meshless method is a synthesis of techniques, suitably adapted, including: spherical harmonic surface interpolation, spectral-element-like integral equation discretization, integral desingularization via variable transformation, and matrix-implicit iterative matrix solution. The spectral accuracy of this combined method is verified using analytically solvable sphere and ellipsoid problems, and then its accuracy and efficiency is demonstrated numerically by solving capacitance and coupled Poisson/linearized Poisson-Boltzmann problems associated with a commonly used model of a molecule in solution. The results demonstrate that for a tolerance of 10^{-3} this new approach reduces the number of unknowns by as much as two orders of magnitude over the more commonly used flat panel methods.

Categories and Subject Descriptors: J.3 [**Computer Applications**]: Life and Medical Sciences—*Biology and genetics*; I.6.5 [**Simulation and Modeling**]: Model Development—*Modeling methodologies*; G.4 [**Mathematics of Computing**]: Mathematical Software—*Algorithm design and analysis*

General Terms: Algorithms, Design, Performance

Additional Key Words and Phrases: Poisson-Boltzmann equation, integral equation, spectral method, meshless

This article is an extended version of the paper “A Spectrally Accurate Integral Equation Solver for Molecular Surface Electrostatics” in Proceedings of the International Conference on Computer-Aided Design (ICCAD’06), 899–906.

The authors acknowledge the support of the MIT-SMA System Biology and BioMEMS programs, the NIH ICBP project, and the National Science Foundation.

Authors’ address: Massachusetts Institute of Technology, 77 Massachusetts Avenue, Cambridge, MA 02139; email: skuo@alum.mit.edu.

Permission to make digital or hard copies of part or all of this work for personal or classroom use is granted without fee provided that copies are not made or distributed for profit or direct commercial advantage and that copies show this notice on the first page or initial screen of a display along with the full citation. Copyrights for components of this work owned by others than ACM must be honored. Abstracting with credit is permitted. To copy otherwise, to republish, to post on servers, to redistribute to lists, or to use any component of this work in other works requires prior specific permission and/or a fee. Permissions may be requested from Publications Dept., ACM, Inc., 2 Penn Plaza, Suite 701, New York, NY 10121-0701 USA, fax +1 (212) 869-0481, or permissions@acm.org. © 2008 ACM 1550-4832/2008/04-ART3 \$5.00. DOI 10.1145/1350763.1350766 <http://doi.acm.org/10.1145/1350763.1350766>

ACM Reference Format:

Kuo, S.-H., Tidor, B., and White, J. 2008. A meshless, spectrally accurate, integral equation solver for molecular surface electrostatics. *ACM J. Emerg. Technol. Comput. Syst.* 4, 2, Article 6 (April 2008), 30 pages. DOI = 10.1145/1350763.1350766 <http://doi.acm.org/10.1145/1350763.1350766>

1. INTRODUCTION

As integrated circuit technology moves to the nanoscale, analysis of molecular-level behavior is becoming a more important tool for designers of new technology. Molecular structure and interactions are determined by a complicated interplay between physical and chemical forces including solvation, electrostatic forces, van der Waals forces, the hydrophobic effect, and covalent bonding. Because of their long-range nature, electrostatic forces are particularly problematic to treat, and both semi-analytic [Qiu et al. 1997; Still et al. 1990; Murray and Politzer 1998] and numerical [Gilson et al. 1985; Sharp and Honig 1990; Davis and McCammon 1990; Grant et al. 2001] techniques have been developed to treat these forces. The result has been an improved understanding of the role of electrostatics in molecular system behavior [Lee and Tidor 2001a], and in particular, has led to techniques for improving ligand-receptor binding affinities by optimizing electrostatic complementarity [Lee and Tidor 2001b]. Although these tools for molecular electrostatics have been most successful in the area of drug design [Kangas and Tidor 2000, 2001; Hendsch et al. 2001], the domain of applications is expanding with the emergence of nanotechnology, and already includes problems such as nanotube sensor design [Kong et al. 2000; Heitzinger 2007].

There are two commonly used approaches to simulating electrostatic effects in systems of molecules, such as systems associated with solvent surrounding a nanotube sensor, or solvent surrounding a receptor-ligand biomolecule complex. One approach is to use atomistic methods such as molecular dynamics [Sharp and Honig 1990; Lounnas et al. 1992; McCammon and Harvey 1987; Brooks et al. 1988; Jean-Charles et al. 1991; Rick and Berne 1994]. In molecular dynamics, all the molecules are tracked individually, including those in the solvent. When large numbers of solvent molecules are needed to insure reasonable accuracy, as is often the case [Stultz 2004], these methods can be extremely time-consuming. A widely used alternative, and the subject of this article, is to use a mixed discrete-continuum approach based on combining a continuum description of the key molecules and solvent with a discrete description of the atomic charges in the key molecules. More specifically, the interiors of the key molecules are approximated as a collection of point charges in a uniform dielectric material, and any surrounding solvent is modeled as a much higher permittivity electrolyte whose behavior is described by the Debye-Hückel theory [Sharp and Honig 1990; Tanford and Kirkwood 1957; Honig and Nicholls 1995; Warwicker and Watson 1982; Madura et al. 1995].

For most molecular systems of interest, the molecular-solvent interface is so geometrically complicated that the electrostatic behavior associated with a mixed discrete-continuum model is usually determined using semianalytic

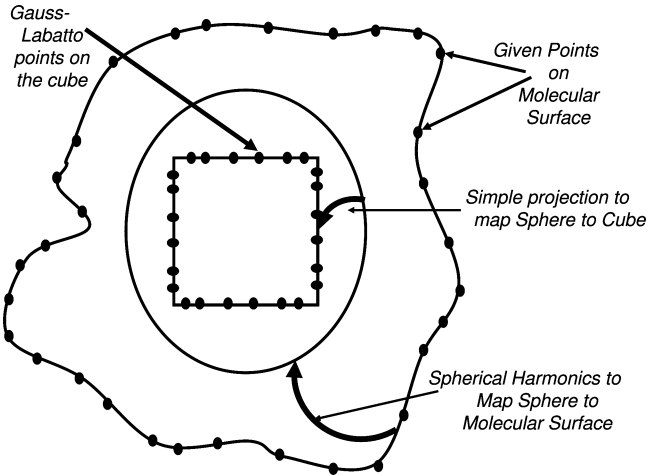


Fig. 1. Summary of meshless approach to molecular surface electrostatics.

approximate techniques based on Borne or generalized Borne radii [Qiu et al. 1997; Still et al. 1990; Murray and Politzer 1998] or by numerically solving the associated coupled Poisson/Poisson-Boltzmann partial differential equations. The commonly used numerical approaches include schemes based on volume discretizations [Gilson et al. 1985; Klapper et al. 1986; Gilson et al. 1987; Nicholls and Honig 1991; Rocchia et al. 2001; Rocchia et al. 2002], or surface discretizations of an integral formulation of the model, in which case linearization of the Poisson-Boltzmann equation plays a central role [Kuo et al. 2002; Yoon and Lenhoff 1990; Zauhar and Morgan 1988; Juffer et al. 1991; Bharadwaj et al. 1995; Zauhar and Varnek 1996; Boschitsch et al. 2002].

Since numerical evaluation of molecular electrostatics are increasingly used in nanotechnology exploration, there is substantial interest in improving their performance [Altman et al. 2006; Lu et al. 2006]. In this article we describe and demonstrate a spectrally accurate integral equation method for electrostatic analysis that is tuned to be extremely efficient for problems involving a certain class of molecular surfaces. In particular, the use of a high-order scheme substantially reduces the number of discretization unknowns needed to meet accuracy requirements for molecular electrostatics, and the problem of reliable generation of molecular surface meshes is avoided by using only *points* on the surface and then interpolating using spherical harmonic expansions.

The diagram of Figure 1 is a summary of the combination of techniques that make up our approach. A least squares method is used to fit a high order spherical harmonic surface representation to the given surface points, and that spherical harmonic surface representation plus simple radial projection are used to construct a differentiable map from the molecular surface to the surface of a cube. A numerically orthogonal basis is generated on each of the rectangular surfaces of the mapped cube, and the coefficients of those basis functions are determined by a Galerkin condition with respect to the surface

integral equation. The integrals which generate the linear system, that is the system which must be solved to enforce the Galerkin condition, are computed using a standard quadrature scheme, after the integrand has been disingularized using a change of variables. Finally, because of the high cost of explicitly forming the required linear system, a matrix-implicit scheme is used to solve for the basis coefficients.

The spectral accuracy of our combined method is verified using analytically solvable sphere and ellipsoid problems, and then demonstrated numerically by solving capacitance and coupled Poisson/Poisson-Boltzmann problems associated with a molecule in solution. The results demonstrate that for a tolerance of 10^{-3} this new approach reduces the number of unknowns by as much as two orders of magnitude over the more commonly used flat panel methods.

The primary contribution of this article is the synthesis of a number of individual techniques, suitably adapted to the molecular surface electrostatics problem. For this reason, there is more background material in this paper than typical, to properly acknowledge contributions to these several techniques. In the next section we describe the background on molecular surface generation, and in Section 3 we describe the least-squares technique used in our method, along with examples to demonstrate the technique's limitations. Background in integral equations and higher-order methods is contained in Section 4, and the detailed techniques used in our spherical-harmonic spectral-element approach are described in Section 5. Implementation details, such as the matrix-implicit solution scheme, are described in Section 6. Results from our implementation in MATLAB[®] are presented in Section 7, followed by conclusions and acknowledgements.

2. MOLECULAR SURFACE REPRESENTATION

For continuum or mixed discrete-continuum models of molecular interactions, there are several commonly used surfaces that serve as interfaces between regions of different electrostatic properties. These surfaces include: the van der Waals surface, the solvent-accessible surface [Lee and Richards 1971] and the molecular surface [Richards 1977; Connolly 1983]. To generate these surfaces, the molecule is represented as the union of solid spheres, one sphere about each atom center in the molecule, and a probe sphere is generated to represent an approaching solvent molecule. The van der Waals surface is the surface generated by the union of the atom spheres in a molecule and is independent of the probe sphere. The solvent-accessible surface is defined much like the van der Waals surface, but with the radii of each atom sphere expanded by the radius of a probe sphere. Alternatively, the solvent-accessible surface can be defined by “rolling” the probe sphere over the surface generated by the union of atom spheres. The boundary defined by the motion of the probe sphere center is the solvent-accessible surface, while the contiguous surface defined by all the points at which the probe sphere is in contact with one or more of the molecule's atoms is defined as the molecular surface. The molecular surface is also known as the solvent-excluded surface. As illustrated in Figure 2, the molecular surface can be described by three analytical shapes: a spherical triangle defined by the

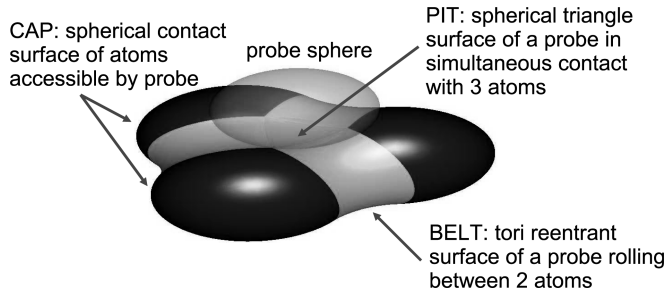


Fig. 2. Molecular Surface.

reentrant surface of the probe sphere when it is in simultaneous contact with three atoms, part of a torus defined by the reentrant surface of the probe sphere when it is in simultaneous contact with two atoms, and part of spherical atoms where the probe sphere can come into direct contact with a single atom. The reentrant surface is defined by the inward-facing surface of the probe sphere as it is in simultaneous contact with more than one atom, and the contact surface is part of the van der Waals surface. Software programs such as MSMS [Sanner et al. 1996] use a molecule's atomic centers and radii, as well as a probe sphere radius, to generate a triangulation of molecular surface, together with other surface properties such as area and normals.

The given implicit surface definition leads to a deceptively simple algorithm for generating large numbers of points on the molecular surface. What may not be clear is the enormous effort required to generate a reliable molecular surface triangulation, or mesh, from the above surface description. The ease of generating surface points and the difficulty generating surface meshes motivated the development of approaches for biomolecule electrostatic analysis that only use surface points.

2.1 Spherical Harmonic Interpolation

Spherical harmonic interpolation, a technique for generating a compact representation of a complete molecular surface from a given collection of surface points, has been used for both for visualization and molecular screening [Leicester et al. 1988; Max and Getzoff 1988; Morris et al. 2005; Duncan and Olson 1993; Brechbühler et al. 1995; Leicester et al. 1994]. To the authors, knowledge, the technique has not been used to generate a numerical technique for solving integral equations.

In the simplest and least general spherical harmonic interpolation scheme, the molecular surface is represented using spherical coordinates, (r, θ, ϕ) , where r is the distance from a selected center point inside the molecular surface, and θ and ϕ are the two rotation angles. If the surface is starlike (explained below), then for any value of θ and ϕ there is a unique value for r so that the triplet is on the molecular surface. In the spherical harmonic interpolation strategy, the function $r(\theta, \phi)$ is approximated using the finite-order spherical harmonic

expansion

$$r(\theta, \phi) \approx \sum_{n=0}^N \sum_{m=-n}^n c_n^m Y_n^m(\theta, \phi), \quad (1)$$

where N is the expansion order, the c_n^m 's are the $(N + 1)^2$ expansion coefficients and are determined from the given collection of surface points, $Y_n^m(\theta, \phi)$ is given by

$$Y_n^m(\theta, \phi) = \begin{cases} N_n^m P_n^m(\cos\theta) \cos m\phi & \text{if } m \geq 0 \\ N_n^{|m|} P_n^{|m|}(\cos\theta) \sin |m|\phi & \text{if } m < 0, \end{cases} \quad (2)$$

where $P_n^m(\theta, \phi)$ are associated Legendre functions, and

$$N_n^m = (-1)^m \sqrt{\frac{(2 - \delta_{0m})(2n + 1)}{4\pi} \frac{(n - m)!}{(n + m)!}} \quad (3)$$

are normalization constants chosen orthonormalize the Y_n^m 's.

To determine the expansion coefficients given a collection of surface points, the standard approach is to start with the formula for the expansion coefficients assuming $r(\theta, \phi)$ is defined for all θ, ϕ . Then the expansion coefficients in (1) are given by

$$c_n^m = \int r(\theta, \phi) Y_n^m(\theta, \phi) d\theta d\phi, \quad (4)$$

as the $Y_n^m(\theta, \phi)$'s are orthonormal functions. The formula in (4) can not be evaluated exactly if $r(\theta, \phi)$ is known only at a collection of surface points, but can be evaluated approximately using fixed-position quadrature. The difficulty is that the accuracy of such constrained quadrature schemes is quite sensitive to point placement [Brechbühler et al. 1995].

It was also noted above that the molecular surface can be represented with a function $r(\theta, \phi)$ only if the surface is starlike [Duncan and Olson 1993]. That is, there must exist an origin within the molecule such that an outgoing ray intersects the molecular surface exactly once, as shown in Figure 3. There are methods that avoid this star-like geometry restriction [Duncan and Olson 1993; Brechbühler et al. 1995; Leicester et al. 1994], and generalize the interpolation approach to any surface that is topologically equivalent to a sphere.

3. LEAST SQUARES SPHERICAL HARMONIC INTERPOLATION

In order to demonstrate that a high-order integral equation solver could be useful for molecular surface electrostatics problems, we chose to use the simple spherical harmonics approach in Equation (1) and accepted the associated geometric limitations. The standard approach to computing the expansion coefficients from a given collection of surface points, applying quadrature to Equation (4), proved to be insufficiently robust, and we used an alternative least-squares approach described below and analyzed by example.

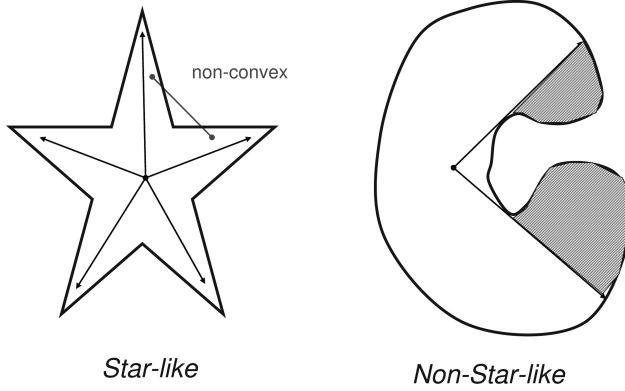


Fig. 3. Molecular surface.

3.1 Least Squares Formulation

In our implementation of a least-squares approach to computing the coefficients in (1), we selected the origin of the spherical coordinate system as the centroid of the given collection of surface points. We also restricted the expansion order, N , so that the number of coefficients in the expansion, $(N + 1)^2$, is much smaller than the number of surface points in the given collection, M . The expansion coefficients are then determined by using the singular value decomposition to solve

$$\min_{\vec{c}} \|\vec{A}\vec{c} - \vec{r}\|, \quad (5)$$

where \vec{c} is the $(N + 1)^2$ -length vector whose entries are the expansion coefficients c_m^n ; \vec{r} is an M -length vector of the given collection of surface points, that is $\vec{r}_i = r(\theta_i, \phi_i)$; and the elements of A are given by

$$A_{i,j} = Y_n^m(\theta_i, \phi_i), \quad (6)$$

where j is index associated with the entry of \vec{c} corresponding with coefficient c_m^n .

Using least-squares to fit a spherical harmonics expansion to a given collection of points on a molecular surface can be quite effective, but has limitations, as the ellipsoid and cusp examples below make clear. This approach can also serve to “smear out” the surface, as demonstrated in the biomolecule example below. The smearing effect can be helpful, as the smeared-out details often contribute little to electrostatic behavior, an observation also made in [Long and Kapur 2000].

3.2 An Ellipsoid

While one can represent an ellipsoidal surface analytically, it is a useful example to demonstrate the effectiveness and the limitation of the spherical harmonic approximation, especially for cases where the shape of the molecular surface is elongated. Figure 4 shows area convergence of spherical harmonic approximation of an ellipsoid with various aspect ratios. As shown in the plot, the larger the aspect ratio, the poorer the spherical harmonic representation for a given

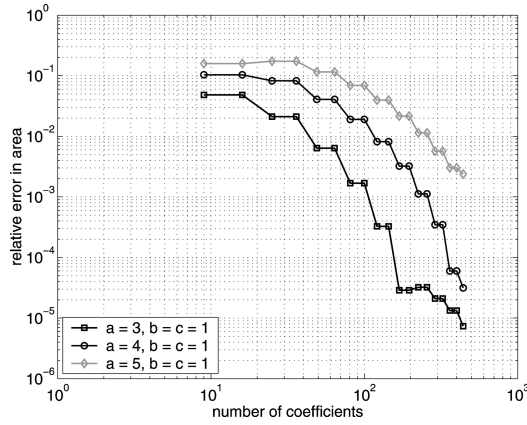


Fig. 4. Area convergence of an ellipsoid using a spherical harmonic approximation.

order and more basis functions have to be used in generating a reasonable approximation. In addition, more surface points will have to be used in generating an expansion of higher order, thus incurring higher computational cost. On the other hand, different strategies [Duncan and Olson 1993] from approximating the radial distance as in (1), or alternative basis such as ellipsoidal harmonics may be useful in representing an elongated surface. But detail studies of those are left for future work.

3.3 A Biomolecule

In order to verify the above method for a general molecular surface, we use the example of a small organic molecule with 26 atoms, the transition state analog (TSA) of the protein enzyme chorismate mutase. The geometry of this small molecule was taken directly from an X-ray crystal structure [Lee et al. 1995], and can be obtained from the Protein Data Bank (PDB) [Berman et al. 2000] as accession number 1ECM. The radii used were 1.0 Å for hydrogens, 1.4 Å for oxygens, 2.0 Å for aliphatic carbons, and 1.7 Å for carbonyl or vinyl carbons. The surface of the TSA molecule was triangulated with the program MSMS [Sanner et al. 1996], using a probe radius of 1.4 Å for water. A spherical harmonic representation is obtained by least squares fit to vertices of the triangulation. Figures 5(c) and 5(d) show an order 5 approximation with 36 coefficients and an order 10 approximation with 121 coefficients respectively for the surface using 3359 points, and a triangulation of 6714 panels. The color in the spherical harmonic surface correspond to the radial distance from the center of expansion, while the color in the triangulated surface correspond to the tori-reentrant, spherical-reentrant and contact surface in the definition of molecular surface. The area of a spherical harmonic surface can be calculated using Equation (25), and is compared to analytical area given by MSMS for increasing order of approximation. In Figure 6, the area convergence versus number of coefficients is shown for three sets of point distributions. The data demonstrates that 5 to 10 times as many points as coefficients can generate a reasonable approximation. For the order 10 expansion, the area error is less

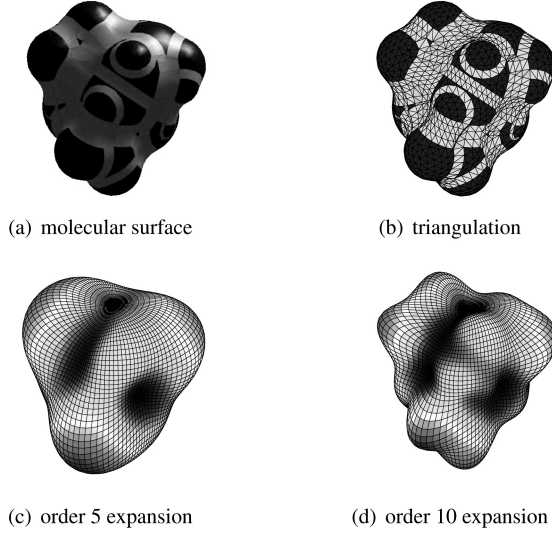


Fig. 5. Geometrical discretization of the TSA molecular surface.

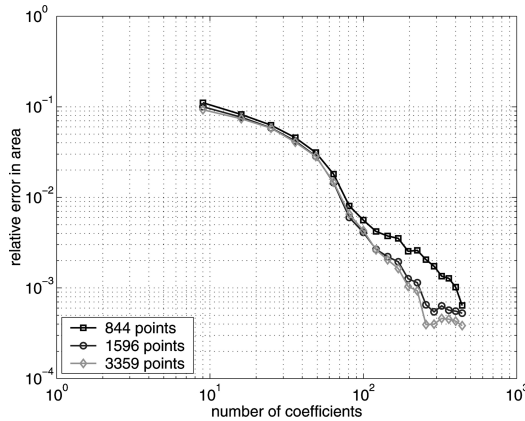


Fig. 6. Area convergence of a TSA molecule using spherical harmonic approximation.

than 0.3%. The convergence seems to stagnate beyond 10^{-3} because MSMS data have precision of three decimal places, which is also the precision given in the experimental data of atomic coordinates.

3.4 The Cusp Problem

In the definition of molecular surface in 2, cusps can sometimes be generated when a probe sphere's reentrant surface intersects with itself. Such an example is shown in Figure 7: a singular edge results when two spherical triangular surfaces intersect each other and two singular vertices result when a tori-reentrant surface intersects with itself. In the case where geometrical singularity exists at a point where normal is not well defined, the global representation using spherical harmonics will not be very effective. This is demonstrated in Figure 8

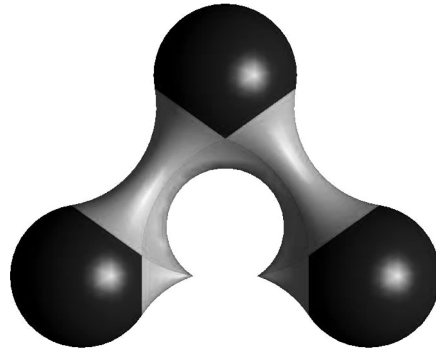


Fig. 7. Geometrical singularities in a molecular surface.

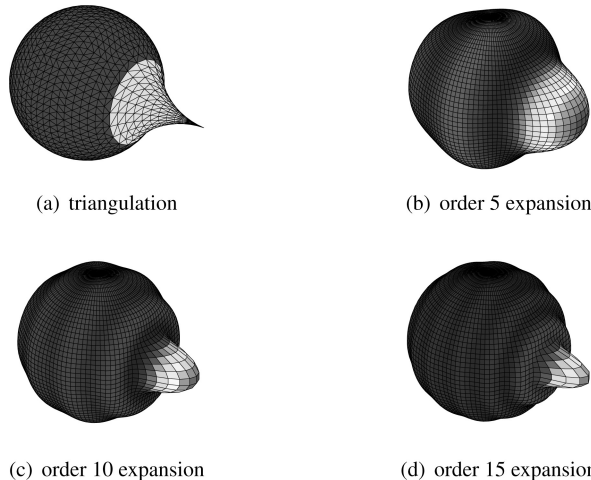


Fig. 8. Spherical harmonic expansion of a smooth surface with one singular vertex.

where in the presence of a singular point in an otherwise smooth surface, the use of triangular panels gives better geometrical approximation than global spherical harmonic representation. As the order of expansion increases, spherical harmonic approximation becomes somewhat better in the smooth region, although ripples, similar to the Gibbs phenomenon, may place a limit on an achievable error tolerance. Furthermore, the expansion fails to capture the singular peak. Such features do not represent an important physical phenomenon, but are an artifact of the definition of the solvent-accessible surface. Such artifacts must be removed by preprocessing [Zauhar and Morgan 1990; Vorobjev and Hermans 1997] before using spherical harmonic expansion.

4. INTEGRAL EQUATION METHODS

Integral equation methods for electrostatic analysis of problems with molecular surfaces are usually formulated with the unknowns on the molecular surface. For example, if the potential ϕ is known on a molecular surface, then a surface charge density σ (possibly fictitious) that will reproduce the exterior field can

be computed by solving

$$\phi(\vec{r}) = \int_{\Omega} G(\vec{r}, \vec{r}') \sigma(\vec{r}') dS', \quad (7)$$

where \vec{r} and \vec{r}' are positions in three-space, Ω is the molecular surface of interest. The kernel, also known as the Greens' function, is denoted $G(\vec{r}, \vec{r}')$ and typically takes one of the following forms depending on the exterior domain:

$$G(\vec{r}, \vec{r}') = \frac{1}{r}, \frac{e^{-\kappa r}}{r} \quad \kappa \in \mathbf{R}, \quad (8)$$

where $r = |\vec{r} - \vec{r}'|$ and is the Euclidean distance. The first kernel in (8) is associated with Laplace's equation, and the second arises in the case of the linearized Poisson-Boltzmann equation. Note that each kernel is singular, that is, each kernel approaches infinity as r approaches zero.

When boundary-element methods [Hess and Smith 1964; Harrington 1968] are used to solve surface integrals with singular kernels, like (7), the associated integral equation is typically discretized using piecewise-constant or piecewise-linear bases on flat panels or triangles, and a system of equations is generated using either a Galerkin or a collocation scheme. The resulting matrix equation is solved iteratively with matrix sparsification techniques [Greengard 1988; Kapur and Long 1997; Hackbusch and Nowak 1989; Beylkin et al. 1991; Rokhlin 1985; Nabors and White 1991; Phillips and White 1997]. This approach has become the method of choice for exterior problems and is used in such diverse applications as interconnect extraction [Tausch and White 1999; Kamon et al. 1994; Zhu et al. 2003], electromagnetic scattering [Song et al. 1997; Jandhyala et al. 1998], MEMS and fluidic simulation [Vassberg 1997; Ramaswamy et al. 1999; Wang et al. 2006; Frangi and di Gioia 2005], and calculating bimolecular solvation energy [Kuo et al. 2002; Altman et al. 2006; Bharadwaj et al. 1995; Zauhar and Varnek 1996; Boschitsch et al. 2002].

Piecewise-constant and piecewise-linear bases are low-order, and flat triangles or panels are poor representations of curved surfaces, and when such discretizations are used on molecular surface problems, very fine discretizations are needed to achieve high accuracy [Bardhan et al. 2007]. While matrix sparsification techniques make it possible to simulate problems with huge numbers of unknowns, the memory requirements eventually present to low an upper limit on the accuracy achievable for complicated geometries. In addition, generating the surface mesh for very complicated problems can be problematic. For these reasons, there is growing interest in finding methods appropriate for molecular surface electrostatic analysis that can both achieve high accuracy with few unknowns (i.e., higher-order methods) and avoid constructing surface meshes (i.e., meshless methods).

4.1 Higher-Order Methods

There is a large body of literature on higher-order methods for solving surface integral equations with singular kernels, but the literature appears in multiple disciplines and can be time-consuming to find. For this reason, and because the method described herein shares features with a number of existing schemes, a

more extensive summary of the literature than typical follows. To organize this summary, we note that most of the methods have been developed from one of two points of view. In one point of view the higher-order method is presented as Nystrom-type; the unknowns are values at surface quadrature points and a special singularity-resolving quadrature scheme is applied. In the second point of view, the method is presented as Galerkin- or collocation-type; the unknowns are coefficients of a higher order basis, though singularity-resolving quadrature also appears. The specialized quadrature schemes are needed to evaluate the equations that enforce the Galerkin or collocation condition.

The most mature of the Nystrom methods were originally developed for two-dimensional problems, where the surface is a curve. A mapping between the circle and the curve is constructed, and then quadrature schemes are developed that exactly integrated products of polynomials and singular kernels over the circle [Kress and Sloan 1993; Kress 1999]. Such globally corrected quadrature schemes interfere with many matrix-sparsification techniques, because distant points contribute in a manner that varies with evaluation point location, though sparsification techniques have been developed for special cases [Tausch 2006]. Locally-corrected quadrature schemes, which can be more easily adapted to matrix sparsification methods, have also been developed [Strain 1995; Gedney 2003; Kapur and Long 1998], but most of these methods rely on accurate evaluation of integrals of products of higher order polynomials with singular kernels, where the domain of integration must be a well-defined “patches” on the surface of interest. Newer methods of this kind attempt to be more meshless [Aluru and Li 2001; Bruno and Kunyansky 2001].

Higher-order Galerkin or collocation methods have a longer history in three-dimensional applications than Nystrom methods [Hess 1979]. Most such methods are similar to spectral element methods for volume problems [Patera 1984] in that the surface is decomposed into elements or patches, and a high order polynomial representation is used to represent the unknowns on each patch. The spectral element theory suggests that such methods should converge *algebraically* with respect to increasing numbers of patches, and *spectrally* with respect to increasing order of the polynomials on each patch, but those convergence rates are only achieved if patch surfaces are also represented to high order [Büchmann 2000; Manier 1995]. This last point is a significant complicating factor, because enforcing the Galerkin or collocation condition requires the time-consuming computation of integrals of products of polynomials and singular kernels over curved surfaces [Wang et al. 2000; Newman 1986].

The higher order approach in the next section is somewhere between Nystrom- and Galerkin-type methods. The method can be considered a Nystrom-type method, because the unknowns are values at points. The method is perhaps more naturally described as of Galerkin type, because there are underlying basis functions, and products of these basis functions with the singular kernel are integrated over curved surfaces.

5. SPHERICAL-HARMONIC SPECTRAL ELEMENT APPROACH

In this section we describe the techniques used in our high-order method for solving surface integral equations with singular kernels on molecular surfaces.

The method requires a global representation of the molecular surface, which we generate from a given collection of surface points using the spherical harmonic expansion method with least-squares fitting described above.

5.1 Numerically Orthogonal Basis

Considering computing an approximation to a density σ on a surface Ω as in the integral equation in (7). The density is often approximated as a weighted combination of basis functions, as in

$$\sigma(\vec{r}) \approx \sum_{i=1}^n \sigma_i B_i(\vec{r}), \quad (9)$$

where the σ_i 's are the basis function weights, and B_i 's are the basis functions.

For piecewise-constant panel methods, $B_i(\vec{r}) = 1$ when \vec{r} is on the i th panel, and is zero otherwise. Note that the panel basis functions are mutually orthogonal, but the resulting representation of σ is piecewise constant and so of very low order. For simple surfaces it is possible to generate a set of basis functions that mostly preserve the orthogonality of the panel method basis functions, but also achieve high order. The approach is to generate a set of polynomials which are orthogonal with respect to a set of quadrature points on the surface. As will be described below, this approach ensures good orthogonality for arbitrarily high order bases, though their supports may have significant overlap.

To derive the formulas for the numerically orthogonal bases, assume that the surface Ω , with coordinates (x, y, z) , can be partitioned into a few regions each of which can be associated with a one-to-one mapping function:

$$P : \vec{r}_{flat}(u, v) \rightarrow \vec{r}_{curve}(x, y, z) \quad (10)$$

defined on a local patch of coordinates (u, v) . In a complicated geometry where exact mapping is not possible, an approximate mapping can be used, but the mapping must be an approximation of order consistent with the basis order, since convergence will be limited by the lower accuracy of the two. A second requirement is that there exist a good set of quadrature points associated with each patch. For a rectangular patch, we selected a tensor product of one-dimensional Gauss-Lobatto quadrature point. The associated basis set can be defined as polynomials that take on unit value at one of the grid points but zero at all other grid points. In one dimension, these are the Lagrangian interpolating polynomials [Berrut and Trefethen 2004]:

$$\ell_i(u) = \frac{\prod_{k=1, k \neq i}^m (u - u_k)}{\prod_{k=1, k \neq i}^m (u_i - u_k)} \quad (11)$$

such that

$$\ell_i(u_k) = \delta_{ik} \quad i, k = 1, \dots, m, \quad (12)$$

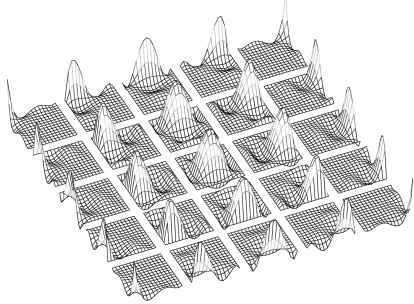


Fig. 9. Two-dimensional Lagrangian basis defined by 5×5 Gauss-Lobatto grid on a patch.

where u_k is coordinate of k th quadrature point. The bases on a patch can therefore be written as a product of two one-dimensional polynomials as in

$$B_{ij}(u, v) = \ell_i(u)\ell_j(v). \quad (13)$$

Therefore, if m quadrature points are used along each dimension, there will be m^2 basis functions. A good set of quadrature points ensures orthogonality as the inner product over a patch approximated by the same quadrature points is always zero by design.

In Figure 9, we show a set of basis functions defined on a patch. Each of the 25 basis takes on unit value at one of the Gauss-Lobatto grid points, and are zero at all other grid points. For the bases associated with a boundary node, the support will span across nearby patches so that computed solutions will be continuous along patch boundaries. The use of such a numerically orthogonal basis was proposed in the spectral element method [Patera 1984] and is well known in the finite element community. However, to authors' knowledge, it has not yet been applied to solving surface integral equations with singular kernels, perhaps hindered by the difficulty of panel integration, the subject of the next section.

5.2 Integration over Curved Surfaces

Once the mapping function (10) and basis functions (13) have been defined on a patch, the integration over the actual surface can be performed using parametric coordinates (u, v) . For an evaluation point at $\vec{r}(x, y, z)$:

$$\int_{(x,y,z)} G(\vec{r}, \vec{r}') B(\vec{r}') dS' = \int_{(u,v)} G(\vec{r}, P(\vec{r}')) B(\vec{r}') |J(\vec{r}')| dS', \quad (14)$$

where $|J|$ is the Jacobian of the mapping function in (10). Note that the basis function, originally defined on the local patch, is also being used to represent the solution in the global surface through the mapping function:

$$B(\vec{r}'(x, y, z)) = B(P(\vec{r}'(u, v))) = B(\vec{r}'(u, v)). \quad (15)$$

An analytical expression for (14) is not generally available, as the Jacobian can be very complicated, and straightforward quadrature in (u, v) coordinates is not sufficiently accurate for evaluation points on or close to the source patch.

It is shown in [Bruno and Kunyansky 2001] that, however, the integral can be de-singularized in appropriately chosen polar coordinates. The key is to locate the origin of polar coordinates such that the radial coordinate ρ goes to zero at the singular point. The resultant integrand is smooth and Gauss quadrature points in (ρ, ϑ) coordinates can be used to evaluate the integral in the collocation matrix:

$$A_{ji,patch}^{Collocation} = \iint_{patch} G(\vec{r}_j, P(\vec{r}'(\rho, \vartheta))) B_i(\rho, \vartheta) |J(\rho, \vartheta)| \rho d\rho d\vartheta, \quad (16)$$

where i and j , unlike in Equations (13), are global indices of all nodes defined on all patches and \vec{r}_j 's are coordinates of collocation points defined by mapping all grid points onto global surface. If the integral is singular, the origin of polar coordinates has to be defined at the local coordinates corresponding to the singular point:

$$(u_o, v_o) = P^{-1}(\vec{r}_j(x, y, z)) \quad \text{if } P^{-1}(\vec{r}_j) \in patch \quad (17)$$

and

$$\begin{aligned} u - u_o &= \rho \cos \vartheta \\ v - v_o &= \rho \sin \vartheta \end{aligned} \quad (18)$$

The inner integral in (16) is evaluated by one-dimensional Gauss quadrature in ρ -coordinate, which in turn is used to evaluate the outer integral, again by using one-dimensional Gauss quadrature in ϑ -coordinate.

The relation between the Gauss-Labatto points used in the integral equation discretization and the Gauss points used to evaluate the desingularized integral is shown for an example case in Figure 10. In the figure, the evaluation point is in the middle of the source patch, and therefore the integral is evaluated by dividing the region in to four triangles. More specifically,

$$\sum_{T=T_1}^{T_4} \int_{\theta_1^T}^{\theta_2^T} \int_0^{\rho(\theta)} G(\vec{r}_{eval}, P(\vec{r}'(\rho, \theta))) B_i(\rho, \theta) |J(\rho, \theta)| \rho d\rho d\theta \quad (19)$$

$$\approx \sum_{T=T_1}^{T_4} \sum_{j=1}^k w_j^T G(\vec{r}_{eval}, P(\vec{r}'(\rho_j, \theta_j))) B_i(\rho_j, \theta_j) |J(\rho_j, \theta_j)| \rho_j. \quad (20)$$

As a final note, if the support for a basis function spans multiple patches, then its contribution to a matrix entry has to be summed up patch-wise, because separate polar coordinates must be used on each patch.

5.3 Jacobian of Spherical Harmonic Surface

In order to incorporate the spherical harmonic representation into the spectral method, one must be able to integrate over the molecular surface given by Equation (1). In addition, in order to de-singularize the integral involving the Green's function, our approach is to carry out the integration patch-wise on six faces of a cube by setting up appropriate polar coordinates on each face. In order to determine the appropriate Jacobian, consider a molecular surface

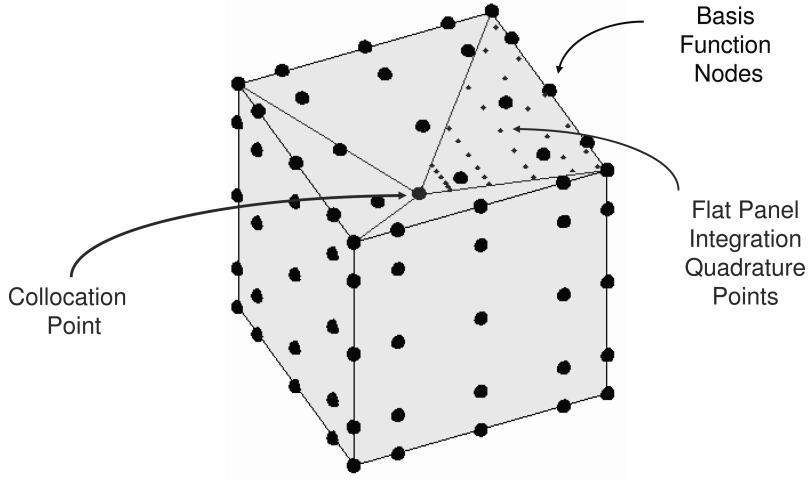


Fig. 10. This figure shows the relation between the integral equation discretization points and the inner quadrature points.

parameterized by θ and ϕ . The normal vector is given by:

$$\hat{N} = \frac{\vec{R}_\theta \times \vec{R}_\phi}{|\vec{R}_\theta \times \vec{R}_\phi|} \quad (21)$$

and the area integral is given by:

$$\int dS = \int_0^{2\pi} \int_0^\pi |\vec{R}_\theta \times \vec{R}_\phi| d\theta d\phi, \quad (22)$$

where

$$\vec{R} = r(\theta, \phi) \sin \theta \cos \phi \hat{x} + r(\theta, \phi) \sin \theta \sin \phi \hat{y} + r(\theta, \phi) \cos \theta \hat{z} \quad (23)$$

\vec{R} is position vector of any point on the molecular surface, \vec{R}_θ and \vec{R}_ϕ are partial derivative of \vec{R} with respect to θ and ϕ respectively. Alternatively, the cross product in Equation (22) can be expressed in spherical coordinates [Garboczi 2002; Baxansky and Kiryati 2005]:

$$\vec{R}_\theta \times \vec{R}_\phi = r^2 \sin \theta \hat{r} - rr_\theta \sin \theta \hat{\theta} - rr_\phi \hat{\phi}, \quad (24)$$

so that

$$\int dS = \int_0^{2\pi} \int_0^\pi r \sqrt{r^2 \sin^2 \theta + r_\theta^2 \sin^2 \theta + r_\phi^2} d\theta d\phi, \quad (25)$$

where $r = r(\theta, \phi)$ in (1), r_θ and r_ϕ are derivatives of radius coordinate with respect to θ and ϕ respectively.

In order to carry out the surface integral on a reference patch on each face of a cube, one needs the Jacobian for the change of variables:

$$d\theta d\phi = |J_{map}| du dv, \quad (26)$$

which corresponds to a mapping from a flat surface parameterized by (u, v) to angular coordinates (θ, ϕ) . Consider the sphere example where $r = r_o$ is constant so that

$$\int_{sphere} dS = \int_0^{2\pi} \int_0^\pi r_o^2 \sin \theta d\theta d\phi = \iint_{cube} \frac{hr_o^2}{(u^2 + v^2 + h^2)^{3/2}} du dv, \quad (27)$$

where h is perpendicular distance from center of sphere to a cube face, one can deduce that

$$|J_{map}| = \frac{h}{\sin \theta(u^2 + v^2 + h^2)^{3/2}} \quad (28)$$

when mapping is along radial direction from center of cube which coincides with center of sphere. We are now in a position to carry out surface integral on reference patches of a cube by combining Equations (25), (26), and (28) where radius function in Equation (1) is represented by spherical harmonics. The evaluation of r and r_ϕ is according to the definition of real spherical harmonics in (2) and r_θ can be calculated utilizing the following relation:

$$\frac{d P_n^m(\cos \theta)}{d \theta} = \frac{(n - |m| + 1)P_{n+1}^{|m|} - (n + 1)\cos \theta P_n^{|m|}}{\sin \theta}. \quad (29)$$

Therefore, when spherical harmonics are used to represent a smooth surface, the Jacobian in (16) is given by

$$|J| = |\vec{R}_\theta \times \vec{R}_\phi| |J_{map}|. \quad (30)$$

5.4 Remark about Galerkin and Collocation Formulations

In the Galerkin formulation in, the outer integral with the target basis is smooth and is typically approximated by quadrature. Since the supports of the basis functions in Equation (13) have been defined on patches associated with quadrature points, one can use the same points to approximate the outer integral:

$$A_{ji}^{Galerkin} \approx \sum_{k=1}^{\#points} w_{j,k} B_j(\vec{r}_{j,k}) |J(\vec{r}_{j,k})| \int G(P(\vec{r}_{j,k}), \vec{r}') B_i(\vec{r}') dS', \quad (31)$$

where i and j are again global indices of all nodes, and k is the index of quadrature points associated with target basis' support, which may be on one or a few patches. So $\vec{r}_{j,k}$ is the position vector of k th quadrature point on B_j 's support with corresponding quadrature weights $w_{j,k}$. Since each basis is chosen to be non-zero at only one quadrature point, each row of the Galerkin matrix in Equation (31) reduces to the corresponding row of the collocation matrix in Equation (16) scaled by some constant. The corresponding right hand side is also scaled by the same constant $w_{j,k} |J(\vec{r}_{j,k})|$. As a result, the Galerkin formulation for the particular choice of basis in Equation (13) is equivalent to the collocation formulation. One can simultaneously take advantage of Galerkin scheme's convergence property and collocation scheme's computational efficiency.

6. MATRIX-IMPLICIT ITERATIVE SOLVER

The cost of constructing the collocation matrix depends on the number of quadrature points used in the polar coordinates. And the use of higher order basis requires a similarly higher order quadrature scheme in order to accurately approximate the integral. The use of quadrature points in computing panel integration tends to dominate the computation time. Since many basis functions share their supports on a patch, an efficient implementation should recycle quadrature points defined on (ρ, θ) among them. This is most easily accomplished when an iterative method is used to solve for the basis function coefficients.

6.1 Implicit Computation

Consider applying the spectral method to solving the example integral Equation (7). If an iterative method is used to compute the basis coefficients, then the matrix-vector product computed in each step of the iterative method will generate potentials from estimated values for the basis coefficients as in

$$\phi(\vec{r}_j) = \sum_{i=1}^n A_{ji}^{Collocation} \sigma_i \quad (32)$$

$$= \sum_{i=1}^n \sigma_i \left(\iint G(\vec{r}_j, \vec{r}'(\rho, \theta)) B_i(\rho, \theta) |J(\rho, \theta)| \rho d\rho d\theta \right) \quad (33)$$

$$= \iint G(\vec{r}_j, \vec{r}'(\rho, \theta)) \left(\sum_{i=1}^n \sigma_i B_i(\rho, \theta) \right) |J(\rho, \theta)| \rho d\rho d\theta \quad (34)$$

where $\sigma_i = \sigma(\vec{r}_i)$ is test solution at collocation points. The summation over all patches within a basis function's support in implicit assumed here. As opposed to a direct solver whereby integration over patches is done for individual basis functions in Equation (33), at each iteration step, a weighted sum of all basis functions in Equation (34) is integrated instead. This is equivalent to first interpolating on each patch via a set of Gauss-Lobatto points, then integrating the interpolated function over the corresponding global surface. In addition to the computing efficiency, an iterative solver uses less memory than a direct solver so larger problems may be solved.

6.2 Performance Compared to Direct Solution

The same efficiency may be achieved with a direct solver, but would require storage of all quadrature points used for panel integration shared among all basis functions on a patch. Since distribution of quadrature points changes depending on location of an evaluation point, this would require storing six sets of quadrature points (for six faces of a cube) for each evaluation point. On the other hand, precomputing and storing the quadrature points could further improve the speed of an iterative solver since no redundant computation needs to be done at each iteration step. Further computational studies on the trade-off between memory and speed should be carried out in a low-level language such as C or C++, but below are performance results based on an implementation

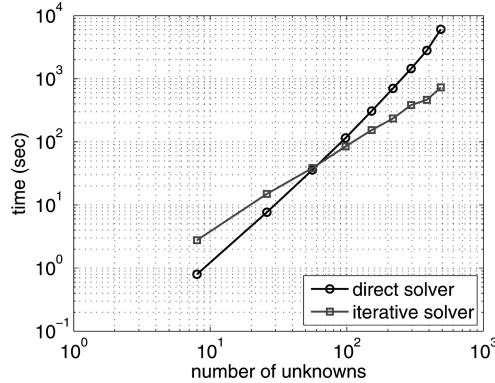


Fig. 11. Efficiency comparison between direct and iterative solver.

Table I. Matrix Condition of Direct and Iterative Solver

order	2	3	4	5	6	7	8	9	10
number of unknowns	8	26	56	98	152	218	296	386	488
condition number	11	32	57	92	136	189	254	327	408
number of iterations	2	5	6	8	8	7	7	5	4

in MATLAB® and optimized for memory: that is, no pre-computing and storing quadrature points for both direct and iterative solvers. Figure 11 shows computation time required for direct and iterative solvers of the sphere example in Section 7.1. The number of iteration required for GMRES [Saad and Schultz 1986] to converge is shown in Table I. Iteration counts stay fairly constant as problem size increases even though no preconditioners are used for the iterative solver. As shown in the figure, computational time for a direct solver grows like $O(n^2)$ where n is number of basis or unknowns. This is because in the implementation in MATLAB®, the cost of panel integration dominates that of Gaussian elimination which has been pre-compiled. On the other hand, if quadrature points are used to integrate a sum of basis functions once per patch per collocation instead of an individual basis function repeatedly, the plot for the iterative solver shows that the cost of panel integration is less than $O(n^2)$. And even though such integration has to be done redundantly at each iteration step, an iterative solver is still faster than a direct solver for all but the smallest problems, when optimized for memory.

6.3 Algorithm Steps

Below we give a summary of all the steps involved in the matrix-vector multiplication used in an iterative solver. We will assume that a spherical harmonic representation of geometry has been obtained, and the basis are defined using Gauss-Lobatto grids on each face of a cube. Given σ_i at collocation points, potentials at evaluation points can be computed as follows:

```
for each collocation point
    for each patch
```

- (1) Choose origin of polar coordinates on a patch according to (17), if evaluation point is on patch. Otherwise, choose the nearest point on patch as the origin.
- (2) Partition patch into triangles by connecting the origin to all vertices. Set up quadrature points in polar coordinates for each triangle.
- (3) Evaluate basis at quadrature points by (11) and (13). The interpolated function at quadrature points are given by (9).
- (4) Evaluate Jacobian at quadrature points by (30), (28), (24) and (1).
- (5) Evaluate Green's function at quadrature points via projection of quadrature points according to (23) and (1).
- (6) Integrate on a reference triangle using the above functional evaluations at quadrature points and appropriate quadrature weights.
- (7) Calculate the integral on a patch in (34) by summing up contribution from each triangle.

```
end
end
```

6.4 Complexity Analysis

To facilitate the complexity discussion, let the number of nodes per side of a square patch be m , so the basis are a set of two-dimensional polynomials of degrees $m - 1$ in each of local (u, v) coordinates. And let the number of quadrature points in polar coordinates used for flat panel integration be k per triangle. Depending on the location of an evaluation point relative to a local patch, the integration may be carried out as a sum over 2, 3, or 4 triangles. The number of quadrature points required for a good approximation to the integral could depend on the order m of the basis functions, as well as the order of an spherical harmonic expansion in the surface representation. To simplify the discussion, however, we will distinguish it with a separate variable and implicitly assume here that k has been chosen large enough to compute the integral to sufficient accuracy.

The dominant cost in the algorithm steps in Section 6.3 are those associated with polynomial interpolation Step 3 and $O(k)$ function evaluations at integration points in Steps 4 and 5. As shown in Berrut and Trefethen [2004], a one-dimensional Lagrangian interpolation costs $O(m)$ per evaluation point. Since the interpolation points are defined on a two-dimensional grid and there are k evaluation points, total cost associated with Step 3 is $O(km^2)$, which is the dominant cost per evaluation point per patch. The number of patches is kept constant at six for mapping from a cube and is small compared to the total number of collocation points, n , so the complexity of the algorithm is $O(knm^2) = O(kn^2)$, same as a straightforward matrix-vector multiplication procedure.

In comparison to a fast solver approach, the asymptotic complexity of the proposed method is less attractive. On the other hand, the number of unknowns needed to achieve good accuracy is a lot fewer with spectral convergence rates than the standard panel method. In such cases, the constant factor associated with the complexity is often more important. A distinct feature of the proposed spectral method is that quadrature points used for panel integration can be

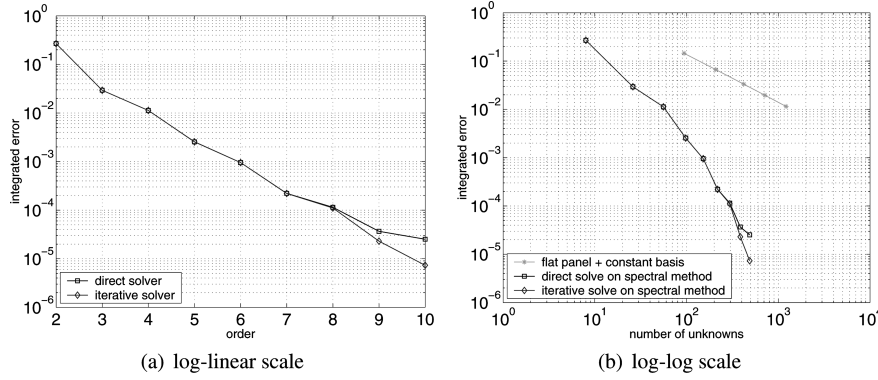


Fig. 12. Accuracy comparison between the standard and spectral method.

shared among many basis functions on a patch, and the number of patches is kept small and constant as number of unknowns increases. This allows the number of calls to a panel integration routine, a costly operation in any boundary element method implementation, to grow only with $O(n)$ as size of basis set increases. In addition, the method's efficiency can be further improved by pre-computing and storing almost all values associated with integration quadrature points (except those interpolated from grid nodes) at the expense of higher memory cost.

7. COMPUTATIONAL RESULTS

7.1 Potential Flow on Sphere

A unit sphere in an infinite fluid potential flow problem, which has an analytical solution [Nabors et al. 1994; Phillips and White 1997], is used to validate the proposed approach. The integral equation in this case is given by

$$\phi(\vec{r}) = \int \frac{\sigma(\vec{r}')}{|\vec{r} - \vec{r}'|} dS'. \quad (35)$$

The spherical geometry can be easily described by a mapping function that radially project any point on a cube to sphere. The Jacobian of the mapping is given in (28). A $m \times m$ Gauss-Lobatto grid is set up on each face of a cube, a set of basis is defined on the grid and $2m \times 2m$ quadrature points in polar coordinates are used to evaluate the integral in (33) or (34).

Accuracy is assessed in terms of integrated error, which is the sum of errors at collocation points, normalized by area. Figure 12 shows the spectral convergence results and a comparison to the standard panel method. Results obtained from a direct solver using Gaussian elimination and an iterative solver using GMRES [Saad and Schultz 1986] are both in display. It can be seen that both direct and iterative solution show similar convergence behavior: a straight line in a log-linear plot and a curve in a log-log plot indicates spectral convergence, and the error decays exponentially with number of unknowns.

As shown in Figure 12(b), the improvement over the traditional approach is clear: not only is the accuracy better for the same degrees of freedom, or

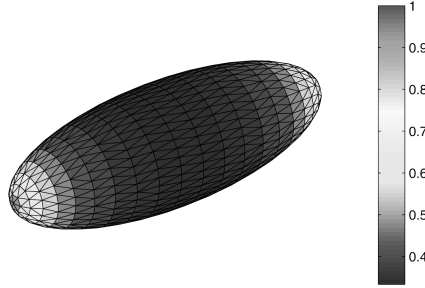


Fig. 13. Charge distribution on an ellipsoidal surface of equal potential.

fewer unknowns needed for the same accuracy, but the method's advantage grows with increasing problem size or more stringent error tolerance. For the sphere problem, the spectral method is able to achieve six digits of accuracy with about 500 unknowns. By extrapolating the straight line, one can estimate that at least a million panels are needed for the standard method to achieve the same accuracy.

7.2 Capacitance of an Ellipsoid

Spherical harmonics can obviously reproduce a sphere exactly, and therefore the above example does not demonstrate the impact of using spherical harmonics to approximate the surface geometry. To test the impact of the geometry approximation, consider the problem of computing the capacitance of an ellipsoid. The ellipsoid has a smooth geometry, but the charge density produced by a constant surface potential is not constant, allowing a meaningful comparison between the spectral and standard methods. The equation of an ellipsoid is given by:

$$\frac{x^2}{a^2} + \frac{y^2}{b^2} + \frac{z^2}{c^2} = 1, \quad (36)$$

where a , b , and c are lengths along its three axes. For simplicity, we will consider the case when two of the lengths are the same ($b = c$), which is a special case of an ellipsoid known as a spheroid. It corresponds to surface of revolution of an ellipse about one of its principal axes. Depending on the axis of rotation, a spheroid can be cigar-shaped (a prolate spheroid) or disk-shaped (an oblate spheroid). Figure 13 shows the test example of a prolate spheroid in the capacitance problem. In the spectral method, local patches are again defined on the six faces of a cube and the Jacobian of the map from a cube to ellipsoid is similar to that of a sphere, but the radial distance R is no longer a constant. The capacitance of a spheroid has an analytical formula [de Queiroz]:

$$C_{prolate} = 4\pi\epsilon_0 \frac{\sqrt{a^2 - b^2}}{\ln \frac{a + \sqrt{a^2 - b^2}}{b}} \quad (37)$$

and Figure 14 shows relative errors in the capacitance calculation of an ellipsoid ($a = 3$, $b = c = 1$) using both spectral method and the standard panel method. As demonstrated in the sphere case, spectral convergence is again validated here from the linear decay in the log-linear plot. The curve in the log-log plot

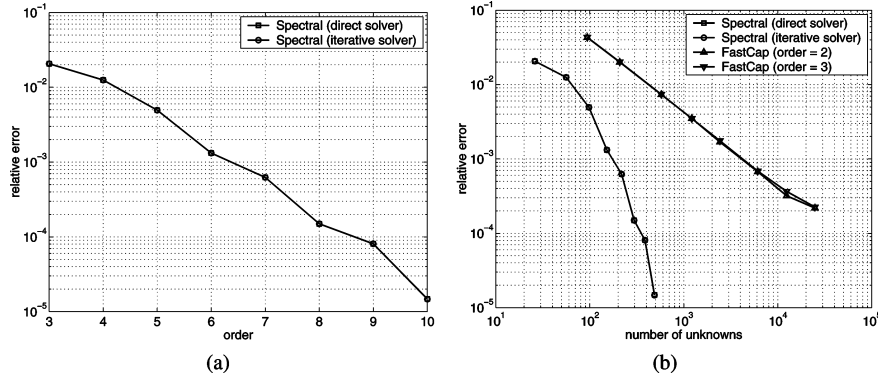


Fig. 14. Capacitance calculation of a spheroid.

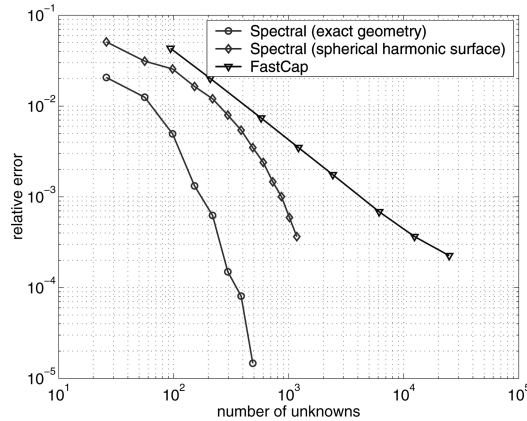


Fig. 15. Capacitance calculation of an ellipsoid.

indicates exponential decay in the error versus number of unknowns. One can compare the improvement in accuracy between both methods in Figures 12 and 14, and note that in the sphere example, the spectral method seems to have a greater improvement over the standard panel method. However, one should also note that the error metrics used in both examples are not equivalent. While the integrated error in the potential flow problem is a sum of absolute errors, the relative error in the capacitance calculation is an error of sums. So depending on the physical quantity of interest, one may achieve a slightly different factor of improvement, but the superior accuracy and convergence in the spectral method is demonstrated in both cases.

Now consider recomputing the capacitance of the ellipsoid, but instead of representing geometry exactly with a mapping Jacobian, a spherical harmonics approximation to the surface is used instead. Figure 15 shows relative errors using the spectral method with exact and approximate geometry, as well as the standard panel method. The plots in Figure 14(b) have been reproduced here for a comparison. An order 15 expansion with 256 coefficients has been used to generate a surface representation which, according to Figure 4, has a relative error

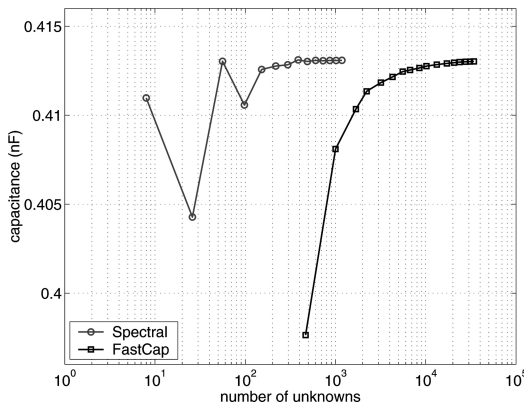


Fig. 16. Capacitance calculation of the TSA molecule.

in area less than 10^{-4} . However, as shown in Figure 15, the error in geometry creates a significant error in the capacitance. Depending on the desired accuracy, a higher-order surface representation may be obtained but the associated computational cost of adopting it in the spectral method will be higher.

7.3 Capacitance of a Spherical Harmonic Surface

In order to verify that our proposed approach works for a general molecular surface, we use the example of a small organic molecule with 26 atoms, the transition state analog (TSA) of the protein enzyme chorismate mutase. The geometry of this small molecule was taken directly from an X-ray crystal structure [Lee et al. 1995], and can be obtained from the Protein Data Bank (PDB) [Berman et al. 2000] as accession number 1ECM. The radii used were 1.0 Å for hydrogens, 1.4 Å for oxygens, 2.0 Å for aliphatic carbons, and 1.7 Å for carbonyl or vinyl carbons. The surface of the TSA molecule was triangulated with the program MSMS [Sanner et al. 1996], using a probe radius of 1.4 Å for water. A spherical harmonic representation is obtained by least squares fit to vertices of the triangulation using 121 spherical harmonic coefficients, and 3359 surface points, and a triangulation of 6714 panels.

Once a spherical harmonic surface is obtained, we can apply the spectral method to solve the integral equation in (35). If the potential is set to unity, the problem corresponds to a capacitance problem. We can therefore compare our method to the standard panel method implemented in FastCap [Nabors and White 1991]. The spherical harmonic surface in Figure 5(d) is used for geometrical representation in the spectral method, and triangulation from MSMS is used to generate input files for the FastCap program. The capacitance calculation for the two solvers with increasing discretization is shown in Figure 16. For the spectral method, the number of unknowns correspond to number of global lagrangian basis used while for the standard panel method, the number of unknowns correspond to number of panels in the triangulation. For the spectral method, the result converge to three significant figures with 386 unknowns

while in the standard method, the same convergence can only be achieved with 27742 unknowns. The spectral method requires almost two orders of magnitude fewer unknowns for a tolerance of 10^{-3} , which is consistent to the observation in the sphere example.

7.4 Solvation Energy of a Biomolecule

For the same TSA molecule, we would like to calculate the solvation energy when it is in an ionic solution. We use the formulation in Kuo et al. [2002] to obtain solution of a linearized Poisson-Boltzmann equation. The coupled integral equations of interest are:

$$\begin{aligned} \frac{1}{2}\varphi_1(\vec{r}_o) + \int_{\Omega} \left[\varphi_1(\vec{r}') \frac{\partial G_1}{\partial n}(\vec{r}_o; \vec{r}') - G_1(\vec{r}_o; \vec{r}') \frac{\partial \varphi_1}{\partial n}(\vec{r}') \right] d\vec{r}' \\ = \sum_{i=1}^{n_c} \frac{q_i}{\epsilon_1} G_1(\vec{r}_o; \vec{r}_i) \end{aligned} \quad (38)$$

and

$$\begin{aligned} \frac{1}{2}\varphi_1(\vec{r}_o) + \int_{\Omega} \left[-\varphi_1(\vec{r}') \frac{\partial G_2}{\partial n}(\vec{r}_o; \vec{r}') + G_2(\vec{r}_o; \vec{r}') \frac{1}{\epsilon} \frac{\partial \varphi_1}{\partial n}(\vec{r}') \right] d\vec{r}' \\ = 0 \end{aligned} \quad (39)$$

where the unknown quantities are potential φ_1 at the dielectric interface and its normal derivative $\frac{\partial \varphi_1}{\partial n}$ on the inner surface. The normal derivatives at the interface has a jump that is related to the relative dielectric constant ϵ . The charge magnitude q_i used can be derived from quantum mechanical calculations. The Green's functions are:

$$G_1(\vec{r}; \vec{r}') = \frac{1}{4\pi |\vec{r} - \vec{r}'|} \quad (40)$$

$$G_2(\vec{r}; \vec{r}') = \frac{e^{-\kappa |\vec{r} - \vec{r}'|}}{4\pi |\vec{r} - \vec{r}'|}, \quad (41)$$

where $\kappa = 0.124 \text{ \AA}^{-1}$, equivalent to an ionic strength of 0.145 M at 25° C was used. A dielectric constant of $4 \epsilon_0$ was used inside the TSA molecule and a dielectric of $80 \epsilon_0$ was used externally. Once the potential and its normal derivative are solved on the molecular surface, potentials everywhere can be calculated. In particular, we are interested in the potential at the charge location. They are known as the reaction potential:

$$\varphi^{REAC}(\vec{r}_i) = \int_{\Omega} \left[G_1(\vec{r}_i; \vec{r}') \frac{\partial \varphi_1}{\partial n}(\vec{r}') - \varphi_1(\vec{r}') \frac{\partial G_1}{\partial n}(\vec{r}_i; \vec{r}') \right] d\vec{r}'. \quad (42)$$

The solvation energy can be calculated by multiplying these potentials with corresponding charge magnitudes.

The spectral method is again compared with the standard panel method implemented with precorrected-FFT acceleration [Phillips and White 1997; Zhu et al. 2003; Kuo et al. 2002]. The results are shown in Figure 17. Note that the size of matrix equation is twice the number of basis shown in the x -axis

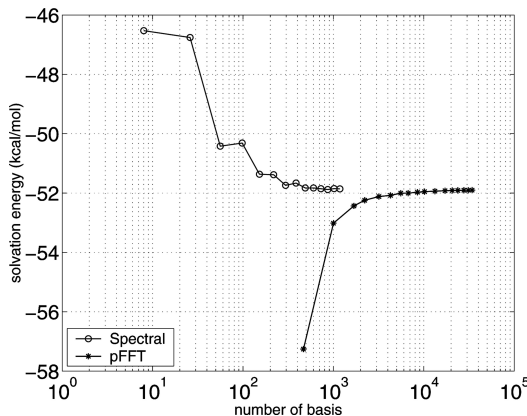


Fig. 17. Solvation energy calculation of the TSA molecule.

since there are two sets of unknowns in the coupled integral equations. This problem is also more challenging due to the presence of double layer potentials. To converge to three significant figures, the spectral method requires 488 basis while the panel method requires 8502 basis. A factor of 20 improvement is obtained with the spectral method.

8. CONCLUSIONS

This article describes a novel approach to discretizing integral equations with singular kernels, such as those associated with electrostatic analysis of molecular surfaces. A spherical harmonic analytic representation of the surface is generated and used to construct a mapping from local patches to the surface, and a global, numerically orthogonal basis is defined on local patches and used to represent the solution. Integration over patches is performed using quadrature after desingularizing with evaluation point specific polar coordinate transformations. The particular choice of polynomial bases results in a reasonably well-conditioned system and the efficient implementation of a Galerkin scheme. The use of a matrix-implicit iterative solver implies that integration over a patch by quadrature need be computed only once per evaluation point. Therefore, the approach is very efficient if the number of patches is small, even if the number of basis functions increases. Computational results demonstrate the method is capable of achieving spectral convergence. When compared to the standard panel method, our approach requires many fewer unknowns for a given accuracy.

It is worth noting that for panel methods, the geometrical discretization and the basis functions are both defined from a single mesh, but geometry and basis functions are decoupled in our spectral method, giving greater flexibility. However, our method requires a global mapping function to describe the surface. For molecular surfaces, the spherical harmonics approach seems to be a promising candidate for creating the mapping, but more work is needed to generalize the mapping to more irregular molecular complexes.

ACKNOWLEDGMENTS

The authors would like to thank Michael Altman and Jay Bardhan for helpful discussions and for providing a software program and examples that were used in some of the comparisons.

REFERENCES

- ALTMAN, M., BARDHAN, J., TIDOR, B., AND WHITE, J. 2006. FFTSVD: A fast multiscale boundary-element method solver suitable for Bio-MEMS and biomolecule simulation. *IEEE Trans. Comput. Aid. Desi. Integr. Circ. Syst.* 25, 274–284.
- ALURU, N. R. AND LI, G. 2001. Finite cloud method: a true meshless technique based on a fixed reproducing kernel approximation. *Int. J. Numer. Meth. Engin.* 50, 2373–2410.
- BARDHAN, J. P., ALTMAN, M. D., WILLIS, D. J., LIPPOW, S. M., TIDOR, B., AND WHITE, J. K. 2007. Numerical integration techniques for curved-element discretizations of molecule-solvent interfaces. *J. Chem. Phys.* 127, 1, 014701.
- BAXANSKY, A. AND KIRYATI, N. 2005. Calculating geometric properties of three-dimensional objects from the spherical harmonic representation. Tech. rep. VIA-2005-6-1, Tel Aviv University.
- BERMAN, H. M., WESTBROOK, J., FENG, Z., GILLILAND, G., BHAT, T. N., WEISSIG, H., SHINDYALOV, I. N., AND BOURNE, P. E. 2000. The Protein Data Bank. *Nucleic Acids Resear.* 28, 1, 235–242.
- BERRUT, J.-P. AND TREFETHEN, L. N. 2004. Barycentric lagrange interpolation. *SIAM Rev.* 46, 3, 501–517.
- BEYLKIN, G., COIFMAN, R., AND ROKHLIN, V. 1991. Fast wavelet transforms and numerical algorithms I. *Comm. Pure Appl. Math.* 44, 141–183.
- BHARADWAJ, R., WINEDEMUTH, A., SRIDHARAN, S., HONIG, B., AND NICHOLLS, A. 1995. The fast multipole boundary element method for molecular electrostatics: An optimal approach for large systems. *J. Comput. Chem.* 16, 898–913.
- BOSCHITSCH, A., FENLEY, M., AND ZHOU, H.-X. 2002. Fast boundary element method for the linear poisson-boltzmann equation. *J. Phy. Chem. B* 106, 10, 2741–2754.
- BRECHBÜHLER, C., GERIG, G., AND KÜBLER, O. 1995. Parametrization of closed surfaces for 3-D shape description. *Comput. Vision Image Underst.* 61, 2, 154–170.
- BROOKS, C. L., KARPLUS, M., AND PETTITT, B. M. 1988. *Proteins: A Theoretical Perspective of Dynamics, Structure and Thermodynamics*. John Wiley & Sons.
- BRUNO, O. AND KUNYANSKY, L. 2001. A fast, high-order algorithm for the solution of surface scattering problems: basic implementation, tests, and applications. *J. Comput. Phys.* 169, 1, 80–110.
- BÜCHMANN, B. 2000. Accuracy and stability of a set of free-surface time-domain boundary element models based on B-splines. *Int. J. Numer. Meth. Fluids* 33, 1, 125–155.
- CONNOLLY, M. L. 1983. Analytical molecular surface calculation. *J. Appl. Crystallography* 16, 548–558.
- DAVIS, M. E. AND McCAMMON, J. A. 1990. Electrostatics in biomolecular structure and dynamics. *Chem. Rev.* 90, 509–521.
- DE QUEIROZ, A. C. M. Capacitance calculations. <http://www.coe.ufrj.br/~acmq/tesla/capcalc.pdf>.
- DUNCAN, B. S. AND OLSON, A. J. 1993. Approximation and characterization of molecular surfaces. *Biopolymers* 33, 2 (Feb.), 219–229.
- FRANGI, A. AND DI GIOIA, A. 2005. Multipole BEM for the evaluation of damping forces on MEMS. *Comput. Mech.* 37, 24–31.
- GARBOCZI, E. J. 2002. Three-dimensional mathematical analysis of particle shape using x-ray tomography and spherical harmonics: Application to aggregates used in concrete. *Cement Concrete Res.* 32, 10 (Oct.), 1621–1638.
- GEDNEY, S. 2003. On deriving a locally corrected Nyström scheme from a quadrature sampled moment method. *IEEE Trans. Antenn. Propag.* 51, 2402–2412.
- GILSON, M. K., RASHIN, A., FINE, R., AND HONIG, B. 1985. On the calculation of electrostatic interactions in proteins. *J. Mole. Bio.* 183, 503–516.
- GILSON, M. K., SHARP, K. A., AND HONIG, B. H. 1987. Calculating the electrostatic potential of molecules in solution: Method and error assessment. *J. Comput. Chem.* 9, 327–335.

- GRANT, J. A., PICKUP, B. T., AND NICHOLLS, A. 2001. A smooth permittivity function for Poisson-Boltzmann solvation methods. *J. Comput. Chem.* 22, 608–640.
- GREENGARD, L. 1988. *The Rapid Evaluation of Potential Fields in Particle Systems*. MIT Press.
- HACKBUSCH, W. AND NOWAK, Z. P. 1989. On the fast matrix multiplication in the boundary element method by panel clustering. *Numerische Mathematik* 54, 463–491.
- HARRINGTON, R. F. 1968. *Field Computation by Moment Methods*. MacMillan.
- HEITZINGER, C. 2007. Computational aspects of the three-dimensional feature-scale simulation of silicon-nanowire field-effect sensors for DNA detection. *J. Comput. Electron.* 6, 387–390.
- HENDSCH, Z. S., NOHAILE, M. J., SAUER, R. T., AND TIDOR, B. 2001. Preferential heterodimer formation via undercompensated electrostatic interactions. *J. Amer. Chem. Soc.* 123, 1264–1265.
- HESS, J. L. 1979. A higher order panel method for three-dimensional potential flow. Tech. rep. McDonald Douglas.
- HESS, J. L. AND SMITH, A. M. O. 1964. Calculation of nonlifting potential flow about arbitrary three-dimensional bodies. *J. Ship Res.* 8, 2, 22–44.
- HONIG, B. AND NICHOLLS, A. 1995. Classical electrostatics in biology and chemistry. *Science* 268, 1144–1149.
- JANDHYALA, V., MICHELSSEN, E., BALASUBRAMANIAM, S., AND CHEW, W. C. 1998. A combined steepest descent-fast multipole algorithm for the fast analysis of three-dimensional scattering by rough surfaces. *IEEE Trans. Geosci. Remote Sens.* 36, 738–748.
- JEAN-CHARLES, A., NICHOLLS, A., SHARP, K., HONIG, B., TEMPCZYK, A., HENDRICKSON, T. F., AND STILL, W. C. 1991. Electrostatic contributions to solvation energies: Comparison of free energy perturbation and continuum calculations. *J. Amer. Chem. Soc.* 113, 1454–1455.
- JUFFER, A. H., BOTTA, E. F. F., KEULEN, B. A. M. V., PLOEG, A. V. D., AND BERENDSEN, H. J. C. 1991. The electric potential of a macromolecule in a solvent: A fundamental approach. *J. Comput. Phys.* 97, 144–171.
- KAMON, M., TSUK, M. J., AND WHITE, J. 1994. FASTHENRY: A multipole-accelerated 3-D inductance extraction program. *Trans. Microw. Theor. Techniq.* 42, 1750–1758.
- KANGAS, E. AND TIDOR, B. 2000. Electrostatic specificity in molecular ligand design. *J. Chem. Phys.* 112, 9120–9131.
- KANGAS, E. AND TIDOR, B. 2001. Electrostatic complementarity at ligand binding sites: Application to chorismate mutase. *J. Phys. Chem.* 105, 880–888.
- KAPUR, S. AND LONG, D. 1998. High-order Nyström schemes for efficient 3-D capacitance extraction. In *Proceedings of the IEEE/ACM International Conference on Computer-Aided Design*. 178–185.
- KAPUR, S. AND LONG, D. E. 1997. IES³: A fast integral equation solver for efficient 3-dimensional extraction. In *Proceedings of the IEEE/ACM International Conference on Computer-Aided Design*. San Jose, CA, 448–455.
- KLAPPER, I., HAGSTROM, R., FINE, R., SHARP, K., AND HONIG, B. 1986. Focusing of electric fields in the active site of Cu-Zn superoxide dismutase: Effects of ionic strength and amino-acid modification. *Proteins: Struc. Func. Genet.* 1, 47–59.
- KONG, J., FRANKLIN, N. R., ZHOU, C., CHAPLINE, M. G., PENG, S., CHO, K., AND DAI, H. 2000. Nanotube molecular wires as chemical sensors. *Science* 287, 5453, 622–625.
- KRESS, R. 1999. *Linear Integral Equations*, 2nd Ed. Springer Verlag.
- KRESS, R. AND SLOAN, I. H. 1993. On the numerical solution of a logarithmic integral equation of the first kind for the Helmholtz equation. *Numer. Math.* 66, 2, 199–214.
- KUO, S. S., ALTMAN, M. D., BARDHAN, J. P., TIDOR, B., AND WHITE, J. K. 2002. Fast methods for simulation of biomolecule electrostatics. In *Proceedings of the IEEE/ACM International Conference on Computer-Aided Design*. San Jose, CA.
- LEE, A. Y., KARPLUS, P. A., GANEM, B., AND CLARDY, J. 1995. Atomic structure of the buried catalytic pocket of escherichia coli chorismate mutase. *J. Amer. Chem. Soc.* 117, 12, 3627–3628.
- LEE, B. AND RICHARDS, F. M. 1971. The interpretation of protein structures: estimation of static accessibility. *J. Mole. Bio.* 55, 379–400.
- LEE, L.-P. AND TIDOR, B. 2001a. Barstar is electrostatically optimized for tight-binding to barnase. *Nature Struc. Biol.* 8, 73–76.
- LEE, L.-P. AND TIDOR, B. 2001b. Optimization of binding electrostatics: Charge complementarity in the barnase-barstar protein complex. *Protein Sci.* 10, 362–377.

- LEICESTER, S., FINNEY, J., AND BYWATER, R. 1994. A quantitative representation of molecular surface shape. I: Theory and development of the method. *J. Math. Chem.* 16, 315–341.
- LEICESTER, S. E., FINNEY, J. L., AND BYWATER, R. P. 1988. Description of molecular surface shape using fourier descriptors. *J. Mole. Graph.* 6, 2, 104–108.
- LONG, D. E. AND KAPUR, S. 2000. Large-scale capacitance calculation. In *Proceedings of the Design Automation Conference*. 744–749.
- LOUNNAS, V., PETTITT, B. M., FINDSEN, L., AND SUBRAMANIAM, S. 1992. A microscopic view of protein solvation. *J. Phys. Chem.* 18, 7157–7159.
- LU, B., CHENG, X., HUANG, J., AND MCCAMMON, J. A. 2006. Order N algorithm for computation of electrostatic interactions in biomolecular systems. In *Proceedings of the National Academics of Science* 103, 51, 19314–19319.
- MADURA, J. D., BRIGGS, J. M., WADE, R. C., DAVIS, M. E., LUTY, B. A., ILIN, A., ANTOSIEWICZ, J., GILSON, M. K., BAGHERI, B., RIDGWAY-SCOTT, L., AND MCCAMMON, J. A. 1995. Electrostatics and diffusion of molecules in solution: Simulations with the University of Houston Brownian Dynamics program. *Comput. Phys. Commu.* 91, 57–95.
- MANIER, H. D. 1995. A three dimensional higher order panel method based on B-splines. Ph.D. thesis, Massachusetts Institute of Technology, Cambridge, MA.
- MAX, N. L. AND GETZOFF, E. D. 1988. Spherical harmonic molecular surfaces. *IEEE Comput. Graph. Appl.* 8, 4, 42–50.
- MCCAMMON, J. A. AND HARVEY, S. C. 1987. *Dynamics of Proteins and Nucleic Acids*. Cambridge University Press, Cambridge, UK.
- MORRIS, R. J., NAJMANOVICH, R. J., KAHRAMAN, A., AND THORNTON, J. M. 2005. Real spherical harmonic expansion coefficients as 3D shape descriptors for protein binding pocket and ligand comparisons. *Bioinformatics* 21, 10 (Feb.), 2347–2355.
- MURRAY, J. S. AND POLITZER, P. 1998. Statistical analysis of the molecular surface electrostatic potential: an approach to describing noncovalent interactions in condensed phases. *J. Molec. Struc.: THEOCHEM, Issues 1–2, Proceedings of the Fifth Annual Conference on Current Trends in Computational Chemistry* 425, 107–114.
- NABORS, K., KORMAYER, F. T., LEIGHTON, F. T., AND WHITE, J. 1994. Preconditioned, adaptive, multipole-accelerated iterative methods for three-dimensional first-kind integral equations of potential theory. *SIAM J. Sci. Comput.* 15, 3, 713–735.
- NABORS, K. AND WHITE, J. 1991. FastCap: A multipole accelerated 3-D capacitance extraction program. *IEEE Trans. Comput. Aid. Des.* 10, 11, 1447–1459.
- NEWMAN, J. N. 1986. Distributions of sources and normal dipoles over a quadrilateral panel. *J. Engin. Math.* 20, 113–126.
- NICHOLLS, A. AND HONIG, B. 1991. A rapid finite difference algorithm, utilizing successive over-relaxation to solve the Poisson-Boltzmann equation. *J. Comput. Chem.* 12, 435–445.
- PATERA, A. T. 1984. A spectral element method for fluid dynamics: Laminar flow in a channel expansion. *J. Comput. Phys.* 54, 468–488.
- PHILLIPS, J. R. AND WHITE, J. K. 1997. A precorrected-FFT method for electrostatic analysis of complicated 3-D structures. *IEEE Trans. Comput.-Aid. Des.* 16, 10 (Oct.), 1059–1072.
- QIU, D., SHENKIN, P. S., HOLLINGER, F. P., AND STILL, W. C. 1997. The GB/SA continuum model for solvation. A fast analytical method for the calculation of approximate Born radii. *J. Phys. Chem. A* 101, 3005–3014.
- RAMASWAMY, D., YE, W., WANG, X., AND WHITE, J. 1999. Fast algorithms for 3-D simulation. *J. Model. Simul. Microsyst.* 1, 1, 77–82.
- RICHARDS, F. M. 1977. Areas, volumes, packing, and protein structure. *Ann. Rev. Biophys. Bioeng.* 6, 151–176.
- RICK, S. W. AND BERNE, B. J. 1994. The aqueous solvation of water: A comparison of continuum methods with molecular dynamics. *J. Amer. Chem. Soc.* 116, 3949–3954.
- ROCCHIA, W., ALEXOV, E., AND HONIG, B. 2001. Extending the applicability of the nonlinear Poisson-Boltzmann equation: Multiple dielectric constants and multivalent ions. *J. Phys. Chem. B* 105, 6507–6514.
- ROCCHIA, W., SRIDHARAN, S., NICHOLLS, A., ALEXOV, E., CHIABRERA, A., AND HONIG, B. 2002. Rapid grid-based construction of the molecular surface and the use of induced surface charge to calculate

- reaction field energies: Applications to the molecular systems and geometric objects. *J. Comput. Chem.* 23, 128–137.
- ROKHLIN, V. 1985. Rapid solution of integral equations of classical potential theory. *J. Comput. Phys.* 60, 187–207.
- SAAD, Y. AND SCHULTZ, M. 1986. GMRES: A generalized minimal residual algorithm for solving nonsymmetric linear systems. *SIAM J. Sci. Stat. Comput.* 7, 856–869.
- SANNER, M., OLSON, A. J., AND SPEHNER, J. C. 1996. Reduced surface: An efficient way to compute molecular surfaces. *Biopolymers* 38, 305–320.
- SHARP, K. A. AND HONIG, B. 1990. Electrostatic interactions in macromolecules: Theory and applications. *Ann. Rev. Biophys. Biophys. Chem.* 19, 301–332.
- SONG, J., LU, C.-C., AND CHEW, W. C. 1997. Multilevel fast multipole algorithm for electromagnetic scattering by large complex objects. *Int. J. Numer. Meth. Engin.* 45, 1488–1493.
- STILL, W. C., TEMPCZYK, A., HAWLEY, R. C., AND HENDRICKSON, T. 1990. Semianalytical treatment of solvation for molecular mechanics and dynamics. *J. Amer. Chem. Soc.* 112, 6127–6129.
- STRAIN, J. 1995. Locally-corrected multidimensional quadrature rules for singular functions. *SIAM J. Sci. Comput.* 16, 4, 992–1017.
- STULTZ, C. 2004. An assessment of potential of mean force calculations with implicit solvent models. *J. Phys. Chem. B* 108, 42, 16525–16532.
- TANFORD, C. AND KIRKWOOD, J. G. 1957. Theory of protein titration curves I. general equations for impenetrable spheres. *J. Amer. Chem. Soc.* 59, 5333–5339.
- TAUSCH, J. 2006. A spectral method for the fast solution of boundary integral formulations of elliptic problems. In *Integral Methods in Science and Engineering*, C. Constanda, Z. Nashed, and D. Rollins, Eds. Birkhäuser Boston, MA, 289–297.
- TAUSCH, J. AND WHITE, J. 1999. A multiscale method for fast capacitance extraction. In *Proceedings of the 36th ACM/IEEE Conference on Design Automation (DAC'99)*. ACM Press, New York, NY, 537–542.
- VASSBERG, J. C. 1997. A fast surface-panel method capable of solving million-element problems. *35th Aerospace Sciences Meeting and Exhibit*, AIAA Paper 97-0168. Reno, NV.
- VOROBIEV, Y. N. AND HERMANS, J. 1997. SIMS: Computation of a smooth invariant molecular surface. *Biophys. J.* 73, 2, 722–732.
- WANG, X., KANAPKA, J., YE, W., ALURU, N. R., AND WHITE, J. 2006. Algorithms in FastStokes and its application to micromachined device simulation. *IEEE Trans. Comput.-Aid. Des. Int. Circ. Syst.* 25, 2, 248–257.
- WANG, X., NEWMAN, J., AND WHITE, J. 2000. Robust algorithms for boundary-element integrals on curved surfaces. In *Proceedings of the International Conference on Modeling and Simulation of Microsystems*. San Diego, CA, 473–476.
- WARWICKER, J. AND WATSON, H. C. 1982. Calculation of the electric potential in the active site cleft due to alpha-helix dipoles. *J. Molec. Biol.* 157, 671–679.
- YOUNG, B. J. AND LENHOFF, A. M. 1990. A boundary element method for molecular electrostatics with electrolyte effects. *J. Comput. Chem.* 11, 1080–1086.
- ZAUHAR, R. J. AND MORGAN, R. S. 1988. The rigorous computation of the molecular electric potential. *J. Comput. Chem.* 9, 171–187.
- ZAUHAR, R. J. AND MORGAN, R. S. 1990. Computing the electric potential of biomolecules: application of a new method of molecular surface triangulation. *J. Comput. Chem.* 11, 5, 603–622.
- ZAUHAR, R. J. AND VARNEK, A. 1996. A fast and space-efficient boundary element method for computing electrostatic and hydration effects in large molecules. *J. Comput. Chem.* 17, 864–877.
- ZHU, Z., SONG, B., AND WHITE, J. 2003. Algorithms in FastImp: A fast and wideband impedance extraction program for complicated 3-D geometries. In *Proceedings of the Design Automation Conference*. Anaheim, CA, 712–717.

Received January 2008; accepted January 2008